Vilnius University
Faculty of Physics

Muhammad Abdullah Tariq

Triboelectric properties of PDMS/SiC composites

Master's final thesis
Electronics and Telecommunication Technologies

Student	Muhammad Abdullah Tariq
Approved	2026-05-22
Academic supervisor	Doc. Martynas Kinka
Director of Institute	prof. Robertas Grigalaitis

Vilnius 2026

Table of Contents

1. Introduction

Triboelectric nanogenerators (TENGs) have emerged as a promising technology for harvesting ambient mechanical energy and powering lightweight electronics, especially for self-powered systems and the Internet of Things (IoT). Their operation relies on the coupling of contact electrification (the triboelectric effect) and electrostatic induction, whereby two materials repeatedly come into contact and separate, generating opposite surface charges and driving current through an external circuit [1].

Among various dielectric polymers, polydimethylsiloxane (PDMS) stands out due to its flexibility, thermal stability, chemical inertness, and ease of fabrication of all crucial characteristics for wearable and flexible TENG devices [2]. However, pure PDMS often has a relatively low dielectric constant, which limits its ability to accumulate high surface charge density and thus reduces the energy output of TENGs [3].

To overcome this limitation, a common strategy is to incorporate high-dielectric fillers such as nanoparticles or nano whiskers into the polymer matrix [4]. Incorporation of SiC to PDMS and SiC@SiO_2 to PVDF composites enhance triboelectric properties. The structure of nanoparticle/whisker helps suppress free- carrier migration and dielectric loss, common issues with bare semiconductor fillers, while still increasing the dielectric constant through strong interfacial effects [3]. This approach enhances the dielectric permittivity of the composite via interfacial polarization at the heterogeneous interfaces, thereby boosting charge separation without compromising the flexibility of the polymer [5].

The aim of this work is to investigate the triboelectric properties of PDMS/SiC composites and their application in developing triboelectric nanogenerators (TENGs) for mechanical energy harvesting. The research will focus on adding silicon carbide (SiC) particles to a polydimethylsiloxane (PDMS) matrix affects its triboelectric behavior, such as its surface charge density, to enhance the output performance of the TENGs, leading to more efficient self-powered electronic systems and sensors by improving the energy harvesting capabilities of PDMS-based TENG devices. The objectives and related tasks are illustrated below.

1. To prepare PDMS and PDMS with silicon carbide in two different morphologies (nanoparticle and nano whisker).

- Prepare Pure PDMS, PDMS/SiC 7%wt and 17.5%wt in nanoparticle.
- Prepare PDMS/SiC with 3.5%wt, 7%wt, 10%wt, 14%wt, 17.5%wt, and 23%wt in nano whiskers.
- These are later laminated over ITO substrate using spin coating.

2. To measure triboelectric properties of prepared samples in vertical contact-separation mode.

- I-V behavior and surface charge density (nC/cm2) will be observed.
- ULOAD and ILOAD will be measured to further analyze the triboelectric behavior of prepared samples with varying load.
- Dissipated power P(RLOAD) will be calculated, and maximum power will be measured for all desired samples, and capacitance in frequency range of 1Hz to 1MHz.

2. Literature Review

2.1 History of TENG

The necessity of low-power and compact electronic devices motivated researchers to develop new energy harvesters. Among various energy harvesting technologies, TENGs have significant reputation due to converting low frequency mechanical energy into electrical energy through triboelectrification and electrostatic induction [6,7]. The phenomenon of triboelectrification has been existing since Greek philosophers observed that rubbed amber can produce light. Although triboelectricity is part of nature, it was practically presented by the development of triboelectric nanogenerator in 2012. In TENGs device, different triboelectric materials with different polarities come into contact, charge transfer occurs during contact and potential difference at the time of separation. With this mechanism, low weight devices could be used to enhance electrical output [8].

The mechanism of triboelectrification is still under discussion. Figure 01, showing the evolution of triboelectricity (from Plato's observations remarks about triboelectric charges are marked as evolution in physics to Carlson's invention of xerographer, which executed triboelectrification in practical world in 1938, Diaz in 1991, making ionomers with controllable triboelectric charging [7]), is basically contact electrification when two materials are charged with physical contact and separation. Triboelectrification and contact electrification are classically approached as identical but they are different. TE between material entails contact electrification and friction. But contact electrification does not require friction for charge propagation (like touching Van de Graaff generator).

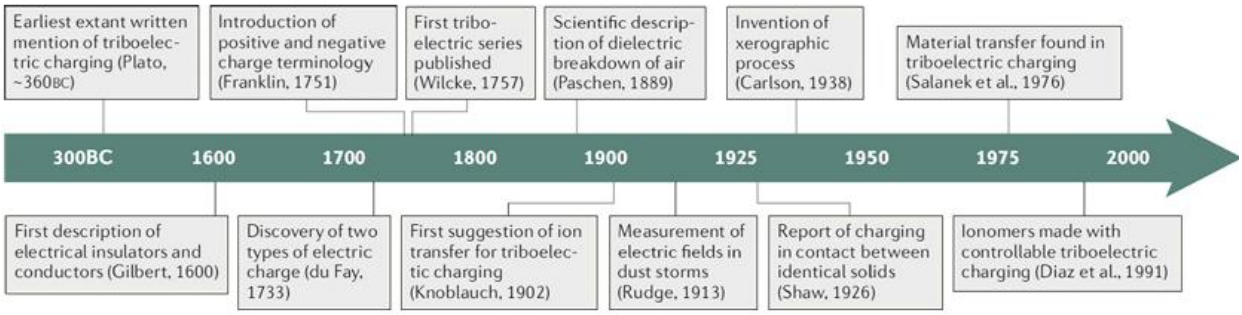

Figure 01: Evolution of Triboelectricity [10]

Researchers helped understanding the importance of charge transfer concept and using initial theoretical concepts to design electronic devices [8]. In 2018, Xu et al. utilized electron transfer mechanism in contact electrification. Their work showed that depending on material's properties, triboelectrification is possible with electron transfer, ion transfer and mass transfer. Their work showed dominance of electron transfer over ion transfer in TENGs [9]. Moreover, Triboelectrification (TE) phenomena can occur in various forms of matters, like solid-solid, solid-liquid, liquid- liquid, solid-gas, liquid gas [10].

In 2017, Wang elucidated that TENGs are flexible power source for daily wear accessories [6]. This sudden shift from laboratory designing to practicality of TENG as a power sensor (achieving comparable output power in contrast with other mechanical energy devices, being flexible and cost-efficient having diversity in material selection), brought huge interest in researchers.

2.2 Types of TENG

As discussed above, Triboelectrification occurs when two materials with varied electric polarities come into contact based on their mechanical motion. After the invention of first TENG device in 2012, output power density mentioned upto 500 W/m^2 with energy conversion efficiency up to 70%. This relates with electrode configuration upon which four different modes of TENG operation are discussed.

2.2.1 Contact-Separation Mode:	In this mode of operation, two different materials with altered polarities come into contact and separate periodically. This contact and separation cause the charge transfer because of different electron affinity and potential difference between both the materials [8]. This mode is used in vertical contact-separation mode which

	we will also use for investigation. It is observed that physical behavior of contact-separation mode can be activated using distance-dependent electric field and 3D mathematical modeling. In addition, change in capacitance under optimal conditions is easier to calculate [10]. Furthermore, Kapton-PDMS contact separation TENGs are also considered crucial as edge effect capacitance for modelling and optimization of the electrical devices [11].
2.2.2 Sliding Mode:	In this mode, altered samples surfaces slide each other in a lateral direction [8]. Overlapping area in this mode changes and electric potential difference occurs at the edges of the dielectric. In contrast with CS mode, this mode of TENG produces more charges [12].
2.2.3 Single-Electrode Mode:	As the name suggests, single-electrode mode involves one electrode attached to ground. Here, the triboelectric layer acts as both charge generating and charge storage layer. In this mode, charges transfer between a triboelectric surface and the moving object which is unattached but not grounded. Single-electron mode is effective in cases where two electrodes cannot be used. for example, generating energy from human walking or vehicle motion [7,8].
2.2.4 Freestanding Triboelectric-Layer Mode:	In freestanding triboelectric layer mode, moveable triboelectric layer is used with two stationary electrodes. In this mode, triboelectric charge generation is decoupled from the electrostatic induction. Freestanding mode is referred to as obtaining high power outputs from rotational motion, also beneficial in fluid dynamics sensing application [8,13].

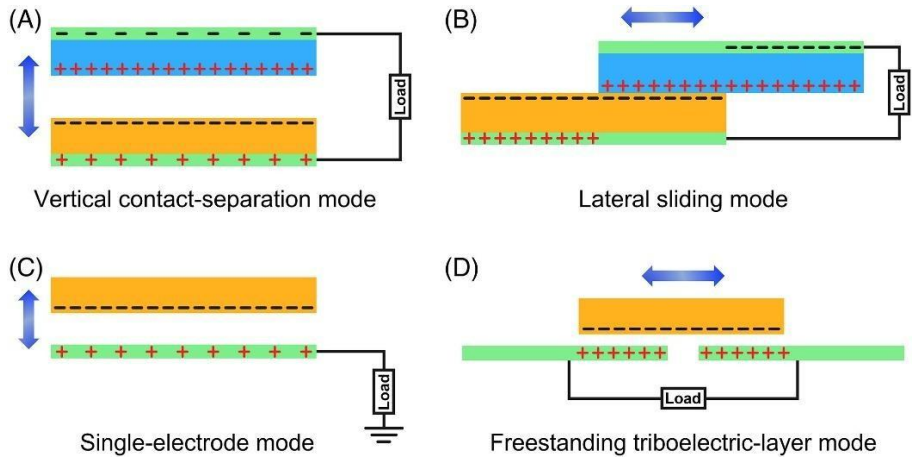

Figure 02: Four Modes of TENG device: (a) Vertical contact-separation mode, (b) Lateral sliding mode, (c) Single electrode mode, and (d) Freestanding triboelectric-layer mode [8].

2.3 Working on Contact Separation

2.3.1 Initial Contact and Charge Transfer:

When two materials with different polarities come into contact, difference in the electron affinity leads to charge transfer. Material with higher electron affinity gains electron becoming negatively charged and the material with lower electron affinity becomes positively charged [7,9]. Xu et al. stated that electron transfer leads the charged generation process in material combinations like polymer-metal or polymer-polymer contacts. The study also illustrated that charge density relies on the contact area, surface roughness, and electron affinity of the materials [9]. Later, Charge transfer process arrives at equilibrium when electric field generated by separated charges becomes stronger enough to stop more electrons from moving. At this point both materials have equal but opposite surface charge densities. For standard triboelectric nanogenerator materials, surface charge density ranges from 100 to 300 $\mu C/m^2$ at room temperature [8].

2.3.2 Separation and Electric Potential Generation:

When the two different charge surfaces are separated, the distance between the two contacts increases and hence the potential difference occurs. If the distance is smaller, maximum value is achieved depending on surface charge density and the device geometry. Slow separation allows better impedance matching but reduces the average output [10]. When the two electrodes join again, potential difference decreases resulting in flowing current in opposite direction (reverse current).

This reverse current flows continuously till next contact occurs. During this phase electrons flow back through the external circuit to decrease the potential electric difference between the two electrodes [7].

2.3.3 Factors Affecting Contact-Separation Performance:

There are numerous factors that affect the performance of contact and separation triboelectric nanogenerator, but surface charge density is the most important parameter which determines the maximum voltage and the current output. This charge density can be modified by using a particular material by increasing the surface area and structural engineering [14]. The separation distance affects the voltage output and the mechanical energy required to withhold that distance. Larger separation distance can cause high voltage, but it also needs more mechanical work which reduces efficiency [10]. Standard separation distance for typical TENG ranges from few millimeters to centimeters [11]. Contact area which evaluates the total charge transferred during each cycle impacts current output. Over the large contact area, current values can be obtained but it can also cause larger mechanical force to maintain uniformity. Contact area can be enlarged through surface texturing and micro structuring [15].

2.4 Theoretical Model of TENG

2.4.1 Expansion of Maxwell equation for TENG:

In TENG device, mechanical movement is coupled with electrostatic induction, which allows surface charges to move through external circuits. This means that when two materials like rubber and metal are pressed together, static charges occur on surfaces. These static charges can act as a source of electricity. Hence, the traditional foundation of contact separation triboelectric nanogenerator depends on the electrostatic principles and Maxwell's equation.

$$\boldsymbol{D = \varepsilon_0 E + P} \qquad (\mathbf{2.4.1})$$

$$\boldsymbol{D = \varepsilon_0 E + P + Ps} \qquad (\mathbf{2.4.2})$$

Where D is total electrical displacement, $\boldsymbol{\varepsilon_0 E}$ represents standard electric field. Wang introduced surface polarization P_s to maxwell equation, because of the existence of electrostatic charges. Since, charge is static, mechanical effort required for conversion, which forms an internal driving force known as displacement current [10].

$$\boldsymbol{J_D = \frac{\partial D}{\partial t} = \varepsilon_0 \frac{\partial E}{\partial t} + \frac{\partial P}{\partial t} + \frac{\partial Ps}{\partial t} = \varepsilon_0 \frac{\partial E}{\partial t} + \frac{\partial Ps}{\partial t}} \qquad (\mathbf{2.4.3})$$

Here, $\boldsymbol{J_D}$ shows total current density generated inside device, $\boldsymbol{\varepsilon_0 \frac{\partial E}{\partial t}}$ shows high frequency current (found in electromagnetic waves) and $\frac{\partial Ps}{\partial t}$ represents mechanical movement current. $\frac{\partial P}{\partial t}$ is neglected, because dielectric polarization is assumed to be changing slowly than P_s. For the addition wang term, the effective volume charge density and current density is updated to;

$$\boldsymbol{\rho' = \rho - \nabla \cdot Ps} \qquad (\mathbf{2.4.4})$$

$$\boldsymbol{J' = J + \frac{\partial Ps}{\partial t}} \qquad (\mathbf{2.4.5})$$

$$\boldsymbol{\nabla \cdot J' + \frac{\partial \rho'}{\partial t} = 0} \qquad (\mathbf{2.4.6})$$

Therefore, maxwell's equation is rewritten in presence of mechanical and electrical interaction.

$$\boldsymbol{\nabla . D' = \rho'} \qquad (\mathbf{2.4.7})$$

$$\boldsymbol{\nabla \times E = -\frac{\partial B}{\partial t}} \qquad (\mathbf{2.4.8})$$

Equation 2.4.7 and 2.4.8 predicts the existence of surface charges which altered the electrodynamic fields without changing the laws of Physics. To bind internal device physics with external circuitry, $\boldsymbol{\phi_{AB}}$ between metal electrode and dielectric material at the bottom of the TENG device is calculated by connecting an external load (Z), and after implementing the displacement current density, internal displacement (I_D) equals to the rate of change of free charges available on electrode.

$$\boldsymbol{\phi_{AB} = \int_A^B E \, . \, dL = \frac{\partial Q}{\partial t} \, Z} \qquad (\mathbf{2.4.9})$$

$$\boldsymbol{I_D = \int J_D \cdot ds = \frac{\partial}{\partial t} \int (\nabla \cdot D) \, d\tau = \frac{\partial}{\partial t} \int \rho \, d\tau = \frac{\partial Q}{\partial t}} \qquad (\mathbf{2.4.10})$$

Equation $\mathbf{2.4.10}$ shows that displacement current is pivoted in optimal conditions and maintains external conduction current through resistive load [10].

2.4.2 Open-Circuit Voltage and Short-Circuit Current:

When two triboelectric surfaces with surface charge density δ separated by distance x as shown in Figure 03, the electric potential difference V_{0C} between the electrodes is expressed as:

$$\boldsymbol{V_{oc} = \frac{\sigma x(t)}{\varepsilon_0}} \qquad (\mathbf{2.4.11})$$

where ε_0 is the permittivity of free space (8.854×10^{-12} F/m). This equation assumes that the triboelectric layers are thin compared to the separation distance and edge effects are negligible [10]. The open-circuit voltage V_{0C} represents the maximum voltage that can be generated when no current flows through the external circuit. This equation shows that V_{0C} increases linearly with separation distance and surface charge density [10]. The short-circuit current I_{sc} represents the maximum current that flows when the electrodes are directly connected with zero resistance. The short-circuit current is related to the rate of change of charge on the electrodes:

$$\boldsymbol{Q_{SC} = \frac{S\,\sigma x(t)}{d_1 + x(t)}} \qquad (2.4.12)$$

$$\boldsymbol{I_{SC} = \frac{dQ_{SC}}{dt} = \frac{\sigma_T\, d_0 S v(t)}{(d_0 + z(t))^2}} \qquad (2.4.13)$$

Here, $\boldsymbol{\sigma_T}$ is total effective surface charge density, $\boldsymbol{d_0}$ is equivalent gap distance, S surface area, and $\boldsymbol{v(t)}$ shows velocity at which two contacts pressed and separated. For sinusoidal motion with frequency f and amplitude x_{max}, the peak short-circuit current can be approximated as:

$$\boldsymbol{I_{SC,Peak} = 2\pi f \sigma A} \qquad (\mathbf{2.4.14})$$

This equation reveals that the short circuit current is proportional to the mechanical frequency, charge density, and contact area [10].

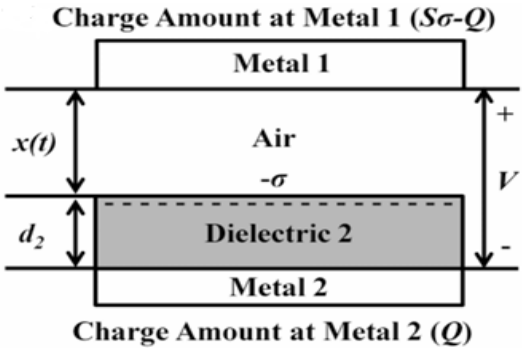

Figure 03: Theoretical model for conductor to dielectric mode for TENG [16]

2.4.3 Power Output and Load Resistance:

The power delivered to an external load resistance RL depends on the impedance matching between the TENG and the load. The instantaneous power P can be expressed as:

$$\boldsymbol{P_{max.} = \frac{V_{0c}^2}{4Z_{TENG}}} \qquad (\mathbf{2.4.15})$$

Where, Z_{TENG} depends on the device capacitance and operating frequency. This relationship guides the design of power management circuits for TENG applications [10]. The energy conversion efficiency $\boldsymbol{\eta}$ of a TENG is defined as the ratio of electrical energy output to mechanical energy input. For a contact-separation TENG, the electrical energy generated per cycle $\boldsymbol{E_{elec}}$ can be calculated by integrating power over one complete cycle:

$$\boldsymbol{E_{elec} = \int_0^T P(t)\ dt} \qquad (\mathbf{2.4.16})$$

The mechanical energy input $\boldsymbol{E_{mech}}$ includes the work required to separate the charged surfaces against the electrostatic attraction force $\boldsymbol{F_e}$:

$$\boldsymbol{E_{mech} = \int_0^{x_{max}} F_e\, dx = \int_0^x \frac{\sigma^2 A}{2\varepsilon_0} dx = \frac{\sigma^2 A x_{max}}{2\varepsilon_0}} \qquad (\mathbf{2.4.17})$$

The energy conversion efficiency is then;

$$\boldsymbol{\eta = \frac{E_{elec}}{E_{mech}}} \qquad (\mathbf{2.4.18})$$

Theoretical analysis shows that efficiency can approach 50-70% under optimal conditions with proper impedance matching, though practical devices typically achieve 10-30% efficiency due to various loss mechanisms [10].

2.4.4 Capacitance Model:

The contact-separation TENG can be considered as a variable capacitor whose capacitance changes with the separation distance. The capacitance C of a parallel-plate configuration is given below:

$$C = \frac{\varepsilon_0 \varepsilon_r A}{d} \qquad (2.4.19)$$

Here, A is the contact area. As the separation distance x increases, the capacitance decreases, and the voltage increases to maintain constant charge [8]. Keykha and Mohammadi emphasized the importance of considering edge-effect capacitance in TENG modeling, particularly for devices with small dimensions or large separation distances [11]. The edge-effect capacitance C_{edge} can be approximated as:

$$C_{edge} \approx \varepsilon_0 \pi L \qquad (2.4.20)$$

Here, L is the perimeter of the electrode. For small devices, this edge capacitance can contribute significantly to the total capacitance [11].

2.5 Strategies to enhance TENG properties

During contact separation between dielectric material and electrode numerous interfacial effects can appear on material surfaces like; adhesion, deformation of prepared samples, fracturing, heat generation, polarization, light and acoustic emission etc., [15]. This can affect charge generation and charge trapping. hence, TENGs performance requires betterment of structural and chemical modifications applicable to PDMS-based devices [14].

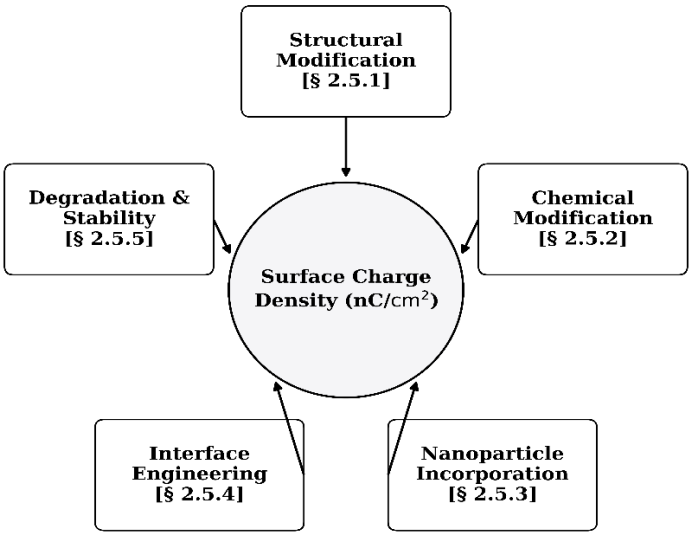

Figure 04: Parameters influencing net surface charge density of dielectric material

2.5.1: Structural Modification:

Structural modification is one of the most crucial techniques for enhancing TENG performance. Nurmakanov et al. showed a comprehensive review of structural modifications, demonstrating that contact area and surface charge density can be enhanced using surface texturing and micro/nano structuring. Lithography technique for micro/nano structing using elastomeric stamps has practically boosted contact area [14]. Common texturing approaches entail pyramid structures, pillar arrays, and hierarchical patterns [17]. Surface texturing creates micro- or nano-scale patterns on the triboelectric surface, which impacts contact area and charge generation. Such texturing increases the effective contact area by factors of 2-5 compared to flat surfaces, eventually impacting charge density and current output [14,17]. Porous structures are another important structural modification. Porous structures of fillers into PDMS or other triboelectric materials increases the effective surface area and changes dielectric properties [17]. This porous structure modification is associated with pore size, distribution, with optimal pore sizes typically in the range of 10-100 μm for PDMS-based TENGs [14].

2.5.2 Chemical Modification:

Šutka et al. analyzed that controlled chemical modification can impact TENG performance. Surface functionalization provides chemical groups which change electron affinity of the triboelectric surface. In case of PDMS, surface functionalization involves plasma treatment, chemical grafting, and self-assembled monolayer deposition. These treatments change the triboelectric polarity, increasing charge density [15].

Chemical doping requires the mixing of electron group (donating or accepting) into triboelectric materials, increasing charge density. However, excess of doped material can cause charge leakage. It is also known that electron accepting polymers have strong electron affinity groups like (-F) and ($-NH_2$) which can increase charge density. TENG materials spread over PET film gave enhanced output [14]. Hence, PET was used] for sample preparation.

2.5.3 Nanoparticle Incorporation:

Incorporating nanomaterials into triboelectric materials is the most impactful technique to enhance TENG performance. Various nanomaterials including metal nanoparticles, carbon

nanomaterials, ceramic nanoparticles, and 2D materials have been added into PDMS and other polymers to influence surface roughness and dielectric properties [18,19].

1D nanostructured materials like nanowires, nanotubes, and nanofibers enhance TENG applications. Machín et al. analyzed 1D nanomaterials like SiC with PDMS, have high aspect ratios, mechanical properties, and ability to enhance charge transfer [18]. 2D nanomaterials like graphene, MoS_2 also performs well in enhancing TENG application. Liu et al. stated that these materials increased charge generation, improved mechanical properties, and enable novel functionalities [19]. Furthermore, researchers said that SiC nanostructures develop surface roughness, resulting in enlarging contact area and generation of charges [14], with dielectric properties increased to 10 with the incorporation of SiC nano whiskers to PDMS.

2.5.4 Interface Engineering:

Interface engineering is concerned with enhancing the properties of the contact interface between triboelectric materials. Šutka et al. proposed that controlling triboelectric surface charge depends on interface properties like surface energy, roughness, and chemical composition. Silane coupling agents functionalize SiC surfaces and improve compatibility with PDMS [15].

Moreover, multi-layer structures of composites can also increase the output performance. Incorporation of different layers into materials with different dielectric properties improves TENG performance with excessive charge storage. However, the thickness and composition of added layer should be optimized for better enhancement [14].

2.5.5 Material Degradation and Stability:

Xu et al. observed the aging effects of PDMS-based TENGs. He analyzed that degradation occurs through multiple mechanisms like surface contamination, charge trapping, mechanical wear, and chemical degradation [20]. Surface contamination occurs through environmental exposure, which results in weakening the charge generation capabilities. This can be prevented through material selection and regular cleaning. Mechanical wear from contact-separation and oxidation, hydrolysis can also occur from long time operation. Degradation in surface structure can be prevented by incorporation of SiC into PDMS [20].

2.6 Material Selection

For high-performance energy applications, material chosen must provide maximum power output

under repeated mechanical cycling. Material selection relates with charge density, triboelectric polarity, dielectric properties and flexibility. One of the prominent TENG includes Polydimethylsiloxane PDMS [17,21].

2.6.1 Triboelectric Series and Material Pairing:

Triboelectric Series ranked materials with their tendency to lose or gain electrons at the time contact-separation. Materials with highest opposite polarities are incorporated to achieve optimized results [7,17]. Zhang and Olin stated that the material incorporation must entail its triboelectric polarity, along with mechanical properties, aging, durability and cost [17]. In triboelectric series, PTFE, FEP, and PVDF are electron acceptors, and aluminum, copper, gold and nylon are electron donors. Fiber-reinforced composites represent an emerging approach for achieving high performance and durability. Liu et al. demonstrated that incorporating fibers impacts mechanical strength and improve energy harvesting efficiency [22].

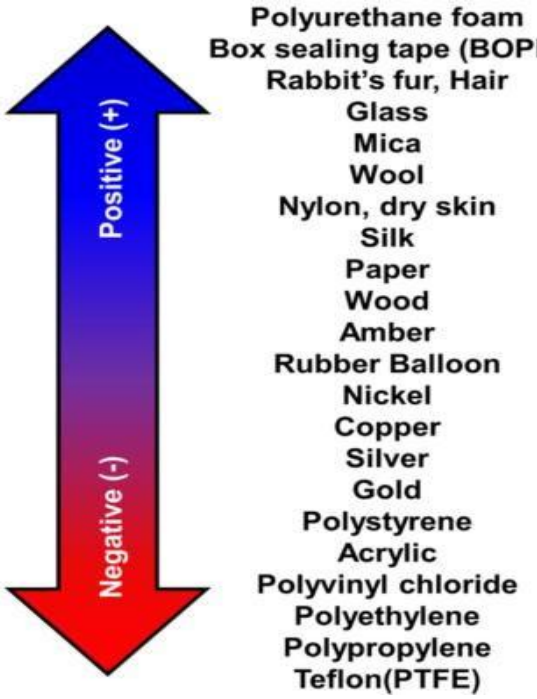

Figure 05: Triboelectric material numbered as their triboelectric charge [14]

2.6.2 PDMS as a Triboelectric Material:

Polydimethylsiloxane (PDMS) has emerged as a widely used triboelectric material because of its

combination of properties. PDMS is a negative triboelectric material in the triboelectric series, making it an effective electron acceptor when paired with metals or positive polymers [17,21]. Kim et al. highlighted several advantages of PDMS [10], including mechanical flexibility, transparent and low-cost processing, biocompatibility, and can accommodate large deformations. PDMS has low dielectric properties of approximately 2.5. This bounds its charge storage capability. Moreover, PDMS surface can contaminate over time reduces the contact area and performance [17].

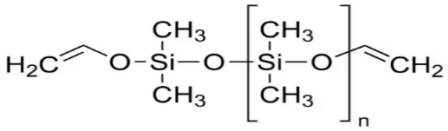

Figure 06: Chemical Formula of PDMS [23]

2.6.3 Silicon Carbide as a Functional Additive:

Silicon Carbide being positive triboelectric material is incorporated with PDMS (with low mechanical strength which limits its performance in high stress application), enhanced PDMS based TENG. SiC has higher dielectric constant in comparison with PDMS [14]. SiC nanoparticles or nano whiskers make surface of the material rough and increase contact area [17]. SiC semiconductor properties may enable photoinduced enhancement effects (in which surface charge can be enhanced and triboelectric polarity of semiconductor material can be reversed through photoexcitation) under UV illumination [24].

2.6.4 Counter-Electrode Material Selection:

The choice of counter-electrode material for PDMS-based TENGs to significantly affect TENG performance, enlist aluminum, copper, and conductive polymers [17,21]. Aluminum being more positive triboelectric polarity than PDMS is widely used, due to its good electrical conductivity, low cost, and ease of processing [17]. The triboelectric polarity difference between PDMS and the counter-electrode produce the maximum charge density. Aluminum-PDMS pairs typically generate charge densities of 50-150 $\mu C/m^2$ under optimal conditions [8]. Moreover, Selection of materials depends upon application requirements. For daily wearables which require durability, biocompatibility make PDMS most suitable for TENG [25]. For fluid sensing applications, PDMS shows chemical resistance, hydrophobicity and

stable triboelectric properties in wet environment [13].

3. Sample Preparation

An adequate quantity of Silicon Carbide was added to the isopropyl solution through sonication (It is a process in which sound waves >20kHz are used to tore down larger particles into smaller equally in a solution) in an ultrasonic bath for 1.5 hours to remove impurities. Later, unrefined PDMS was added to the SiC /IPA solution, and the resulting mixture was subjected to an additional 3 hours of sonication.

As discussed above, that sample will be prepared in two different morphologies (nanoparticles and nanofiber). These altered morphologies are associated with silicon carbide which is incorporated in polydimethylsiloxane. PDMS utilized for sample preparation are sourced from Sigma-Aldrich, which is a U.S based corporation operating globally for nanomaterials selling. Sylgard 184,1 PDMS resides upon two components polymeric base and a curing agent, having weight ratio 10:1 and tensile strength of ~5.2 MPa at optimum condition [23]. Furthermore, impurity silicon carbide (CAS No. 409-21-2) nanofiber is also acquired from Sigma-Aldrich. Its specification enlists; diameter < 2.5μm, aspect ratio ≥ 20, and 98% trace metals basis.

The slurry of SiC/PDMS was deposited on IOT-PET substrate surface using spin coating technique. Spin coating is a technique used to apply uniform thin films onto a substrate by spinning it at high speeds while dispensing a liquid solution. The centrifugal force spreads the liquid evenly, and the solvent evaporates, leaving behind a controlled film thickness. For spin coating, 150i spin coater is used, having high precision and better film deposition. The spin speed is 800rpm which helps to thick the layer. A higher spin time of 120s is taken for evaporation of solvent and even liquid spreading. After spin coating, the material (PDMS, PDMS and SiC 7%, and PDMS and SiC 17.5%) are cured at 110◦C for 3 hours. After sample preparation, thickness of all three substrates was calculated. For Pure PDMS thickness is 0.10mm, PDMS and SiC 7% (nanoparticle) is 0.14mm, and PDMS and SiC 17.5% (nanoparticle) is 0.35mm thick, PDMS and SiC 7% (nanofiber) is 0.17mm, and PDMS and SiC 17.5% (nanofiber) is 0.13mm.

To evaporate the IPA, the SiC/IPA/PDMS suspension was placed on a hot plate magnetic stirrer at 80◦C and left for several hours. A curing agent in a 1:10 ratio to PDMS was introduced into the PDMS mixture, followed by gentle manual stirring for 10 minutes. The resulting SiC/PDMS/hardener slurry is now ready for further casting manipulations and final curing. This slurry is quantized in three concentrations, Pure PDMS, PDMS with 7% of SiC and PDMS with

17.5% SiC, which according to the research requirements. ITO PET (Indium Tin Oxide on Polyethylene Terephthalate) sheets of area 2.5 × 2.5 cm2 were used as substrate. These are widely used due to their transparency and property of electrical conductivity. These properties make it a suitable substrate to be used for TENG applications. Additionally, Polyethylene Terephthalate provides mechanical support to Indium Tin Oxide.

Table # 01: Concentrations and Thicknesses of Prepared Samples

Sample	Concentration (% wt)	Thickness (mm)
Pure PDMS	0	0.10
PDMS/SiC$_p$	7	0.14
PDMS/SiC$_p$	17.5	0.35
PDMS/SiC$_w$	3.5	0.083
PDMS/SiC$_w$	7	0.11
PDMS/SiC$_w$	10	0.11
PDMS/SiC$_w$	14	0.108
PDMS/SiC$_w$	17.5	0.12
PDMS/SiC$_w$	23	0.15

4. Methodology

For analyzing triboelectric properties of the prepared samples (Pure PDMS, PDMS and SiC (nanoparticle and nano whisker) were performed using the contact devices in figure 4. Contact device has an electromagnet on top. This electromagnet relates to the top contact (tip) of the contact device which is aluminum in this work. Moreover, Aluminum is connected to positive terminals of the power supply. At the bottom, prepared sample (Pure PDMS, PDMS and SiC (nanoparticles and nanofiber) is adjusted. The negative terminal of power supply relates to bottom contact.

This vertical contact separation mode works when a 20N force is applied, Aluminum tip with the

circular area of 2cm^2. The primary electrical outputs (VOC and ISC) and the load-dependent current/voltage measurements were captured via a Tektronix TDS 2024B digital oscilloscope and a Keithley 6514 electrometer.

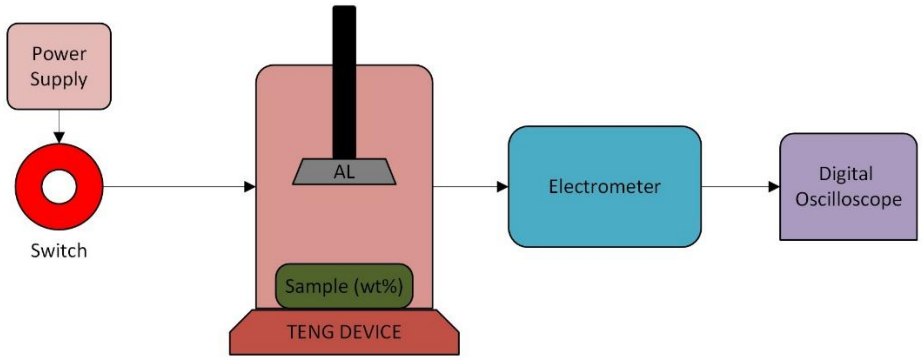

Figure 07: Schematic Diagram for Measuring

The TENGs performance was systematically analyzed across a load spectrum from 100 kΩ to 500 GΩ (21 distinct resistors). To optimize measurement collection when the load applied on Pure PDMS, PDMS and SiC with 7% and 17.5% nanoparticle, 20% contact symmetry was applied to low-resistance loads, while high-resistance measurements were evaluated at 50% symmetry. For PDMS and SiC with 7% and 17.5% nanofiber, contact symmetry was fixed at 50%. Finally, dielectric properties were studied via capacitance measurements across a frequency spectrum of 20 Hz to 1 MHz using a high-precision HP4284A LCR meter. These measurements are crucial for understanding the dielectric constant's influence on charge-trapping density and overall performance enhancement in the SiC-doped devices.

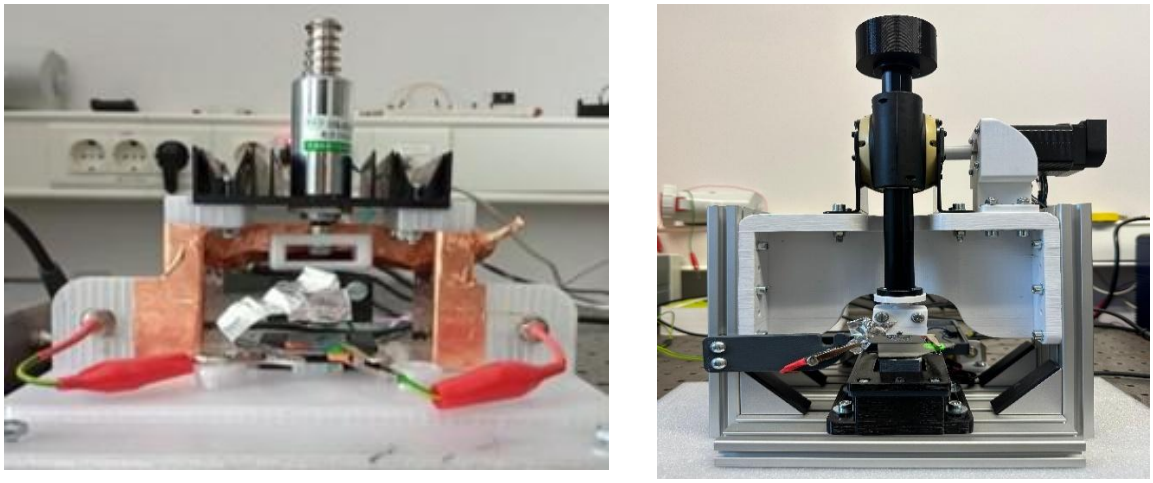

(a) (b)

Figure 08: Contact Devices

Contact device (b) shown in figure 4, utilized to perform triboelectrification with 11N force applied on prepared PDMS/SiC whiskers ranging from 3.5 wt% to 23wt%. Moreover, the time of contact and separation is 100ms, keeping the distance of 4mm when separating from bottom of the TENG. In addition, U_{Load} and I_{Load} were measured at varying load with the at 0N force condition as initial stage on multichannel software, so that 11N could be visible at the digital oscilloscope at the time of contact and 0N at the time of separation between top and bottom contact. Capacitive behavior for prepared PDMS/SiC whiskers ranging from 3.5 wt% to 23wt% was analyzed using impedance meter in the same frequency range.

5. Experimental results and Discussion

5.1 Nanoparticle vs. Nano whisker:

The graph in Figure 10 elucidates the peak voltages for all five samples achieved in open circuit mechanism. In the graphs, black peaks represent Pure PDMS with the peak voltage of 83V, PDMS with SiC 7% nanoparticle is represented with red color and voltage ranges at 70.9V, PDMS with SiC 17.5% nanoparticle has green color with 70.69V, PDMS with SiC 7% nanofiber with blue color has voltage value at 87.35V, and PDMS with SiC 17.5% has cyan color with maximum voltage of 93.442V. It also shows the points of peaks and falls, which occurred when Al as top contact and Pure PDMS, and PDMS with nanoparticle and nanofiber SiC 7% and 17.5% as bottom contact separated and contacted at certain times with certain conditions. Maximum potential difference occurs at the time of separation between two layers. A difference has been witnessed since the maximum voltage achieved at 93.422V after using

nanofiber at the concentration of 17.5% SiC with PDMS. Pure PDMS has stable peaks of voltage. Surface potential increased because SiC along with PDMS increased the charge trapping capability. These graphs also clear that nanofiber brought highest potential difference in comparison with nanoparticles of SiC. Moreover, Voltage decreases with higher concentration of SiC in both morphologies. Open circuit voltage values attained, are instantaneous value take over a time interval. Voltage is measured in parallel and shown in Figure 09.

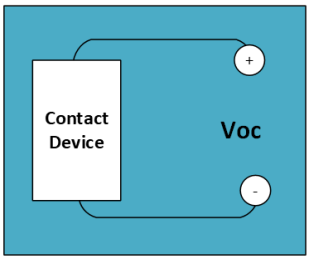

Figure 09: Circuit Diagram of Open Circuit Voltage

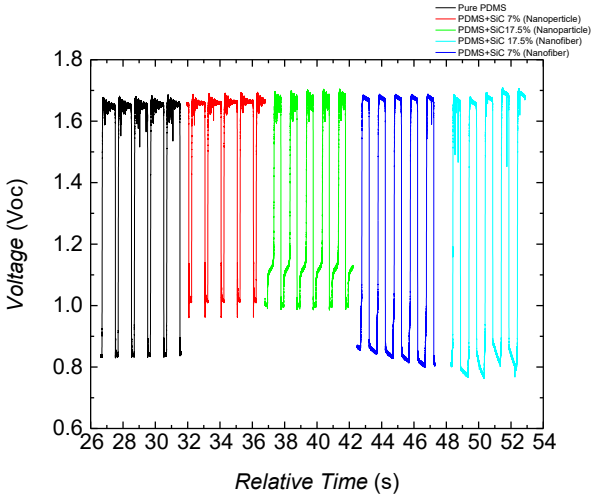

Figure 10: Open circuit voltage

Short Circuit is measured in series as shown in Figure 11. Figure 12 below elucidates the difference of the charge transfer happens while using Pure PDMS, Nanoparticle and Nanofiber PDMS + SiC with 7 % and 17.5%. All the five curves have the same color mechanism used for open circuit voltage peaks. Pure PDMS (Black color curve) gave highest short circuit current value at 1.5957uA, PDMS with SiC 7% nanoparticle (Red color curve) has Isc value at 1.3798uA, PDMS with SiC 17.5% nanoparticle (green color) has 1.4082uA. In case of nanofibers, PDMS with SiC 7% has second highest at 1.4570uA and lowest value for PDMS with SiC 17.5% has 1.0546uA.

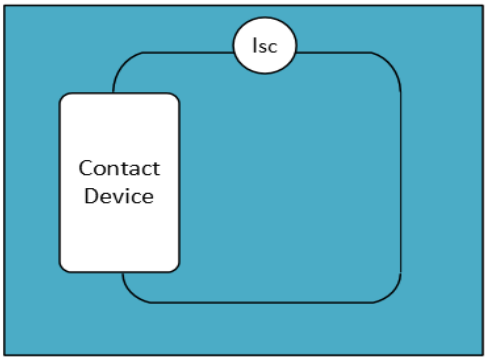

Figure 11: Circuit Diagram for Short Circuit Current Measurement

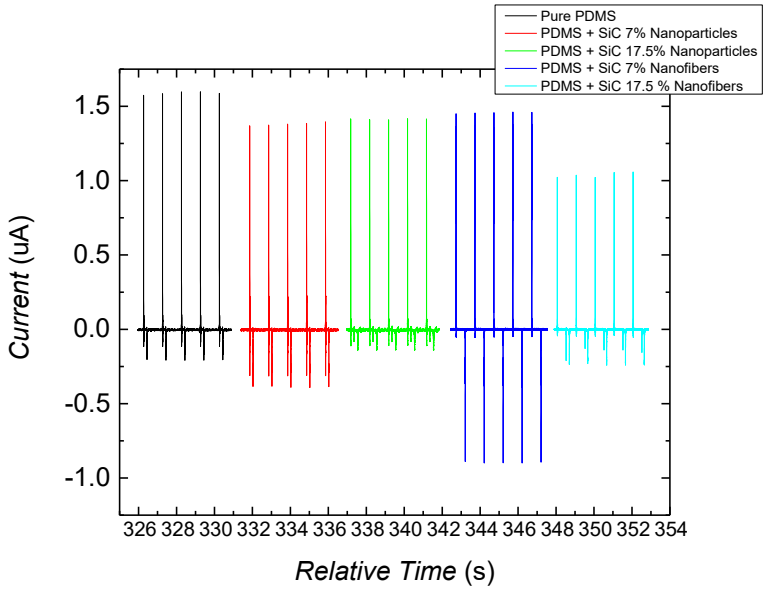

Figure 12: Short Circuit Current

In this case, when the upper and bottom layer come into contact, charges flow to bottom and current peaks become visible. At the time of the contact, due to flexible nature of PDMS, surface charge density also increases. The graph confirms the Plyushch et al. [6] work which suggests that nanofiber provides more conductive pathways as compared to spherical nanoparticles. But, by elucidating the graph further, it also tells us that the nanofiber with 17.5% composites of SiC with PDMS (wider) does not provide higher peak like the other nanofiber.

Surface charge density, one of the crucial parameters to analyze the performance of TENG materials, is obtained by applying integration on short circuit current values with relative time. Later, area retrieved from integration is divided by 2 cm^2 for Q (both positive and negative values)

performed on origin pro. From the graph shown below, it illustrates that surface charge density increases with increase in Silicon Carbide concentration in PDMS. The equations utilized in finding charge density are illustrated below along with the table.

$$\delta = \frac{Q}{A} \qquad (5.1)$$

Where, Q is the total triboelectric charge, σ is the surface charge density, and A is the contact area. This equation highlights why increasing surface area through nano structuring and boosting charge density through material selection are critical for TENG performance.

$$\mathbf{Q} = \int I_{SC}\, dt \qquad \mathbf{(5.2)}$$

$$\delta = \frac{1}{A}\int I_{SC}\, dt \qquad \mathbf{(5.3)}$$

Table 2: Surface Charge Density

Samples	Q(+ve) nC/cm^2	Q(-ve) nC/cm^2
Pure PDMS	1.647	-1.77
PDMS +SiC$_p$ 7%	2.046	-1.7
PDMS + SiC$_p$ 17.5%	2.18	-1.88
PDMS + SiC$_w$ 7%	2.56	-3.31
PDMS + SiC$_w$ 17.5%	1.072	-1.56

Nanofiber brought highest charge value of 2.56 nC/cm^2 and -3.31 nC/cm^2. This higher value of Q for Nanofibers is due to higher surface-area-to-volume ratio, which creates more heterogeneous interfaces for interfacial polarization. Following the previous results of the 17.5% Nanofiber sample, the charge density dropped to 1.072 nC/cm^2. This phenomenon suggests charge leakage instead of storage, eventually reducing the net surface charge.

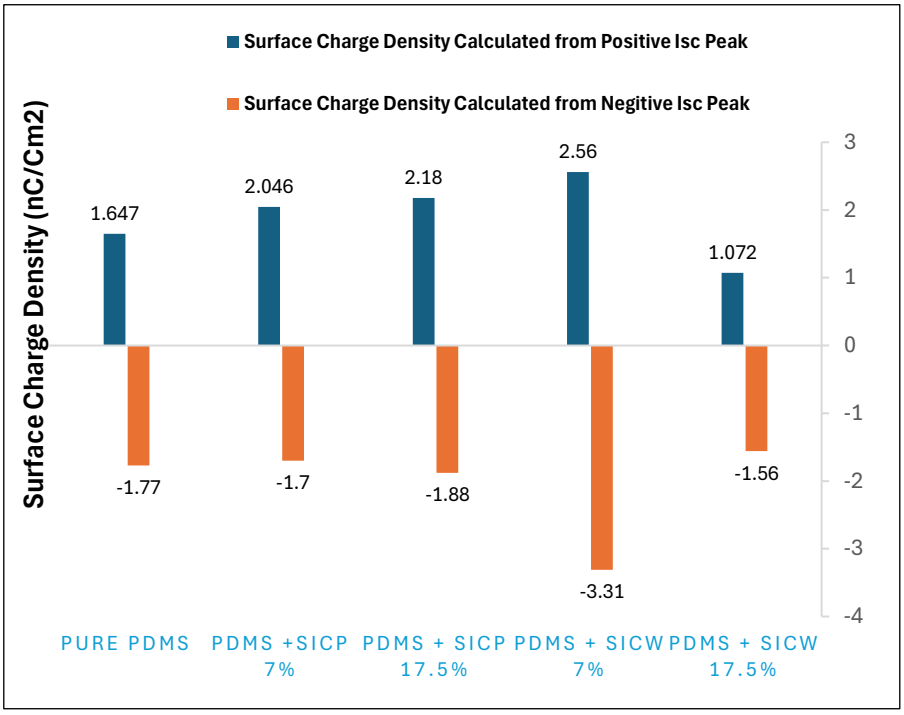

Figure 13: Surface Charge Density

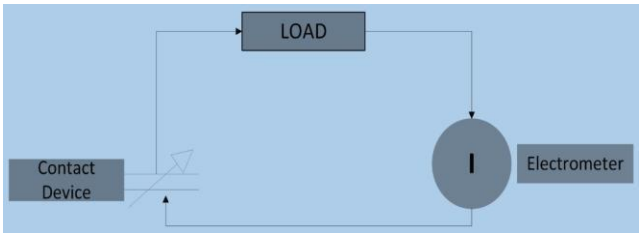

Figure 14: Circuit Diagram for Load Current Measurement

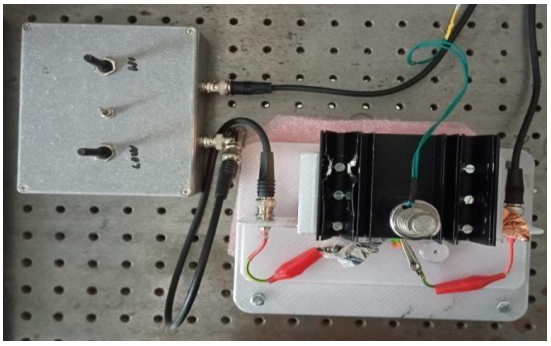

Figure 15: Load Current Apparatus

The graph for load current (Figure 16) and voltage (Figure 17) is created by applying external resistance to contact device (top contact is connected positive side of the load and substrate the

bottom contact relates to negative part). As shown in the image, the resistive load has two tunning sides from low resistances to high resistances. For load measurement, symmetries were changed on the multi-channel software. For low resistance, it is tuned at 20% and for high resistance at 50%. And, at different resistance values, RMS values of current are taken, these RMS peaks show how current is increasing at lower resistance at start and how it falls to lower value at higher resistance. possibly increasing conductivity slightly but reducing the effective charge buildup needed for higher voltage generation. At high resistance, charge transport is limited by internal resistance of the composite. Pure PDMS has high internal resistance and addition of silicon carbide reduces internal resistance.

I(R) for PDMS with SiC 7 (Nanofiber) is 0.104uA > I(R) for PDMS with SiC 7% (Nanoparticle) is 0.061uA > I(R) for PDMS with SiC 17.5% (Nanofiber) is 0.053uA > I(R) for Pure PDMS is 0.041uA > I(R) for PDMS with SiC 17.5% (Nanoparticle) is 0.0042uA.

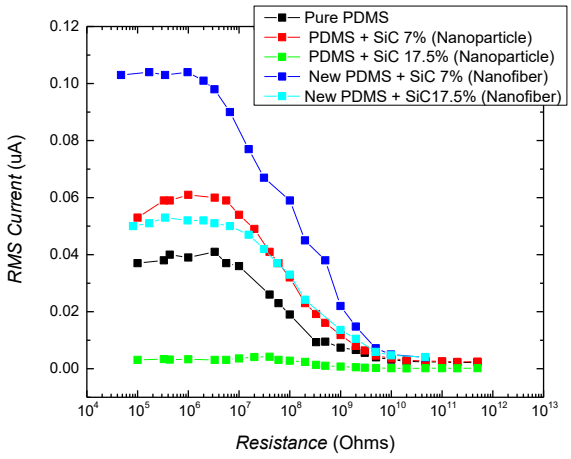

Figure 16: Load Current RMS

For load voltage RMS values, load resistance is varied the same as in case of load current, following its ideal nature. It showed how at lower resistance, RMS values were lower and how high resistance arose the peak due to better charge separation in Silicon Carbide in comparison with Pure PDMS. Likewise, the load voltage is measured in parallel. The lowest value of resistance is 100kΩ and highest value for the load is 700GΩ. In addition, PDMS with SiC (Nanoparticle) 17.5% sample reading for both load voltage and load current were measured without applying weight (135g), because, at high resistance sample started sticking with the upper contact (Al), due to flexibility of PDMS. Moreover, PDMS with SiC 7% and 17.5% (Nanofibers)

were used by applying weight to measure load voltage.

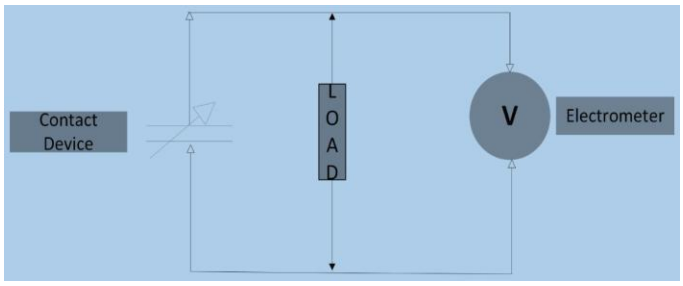

Figure 15: Circuit Diagram of Load Voltage

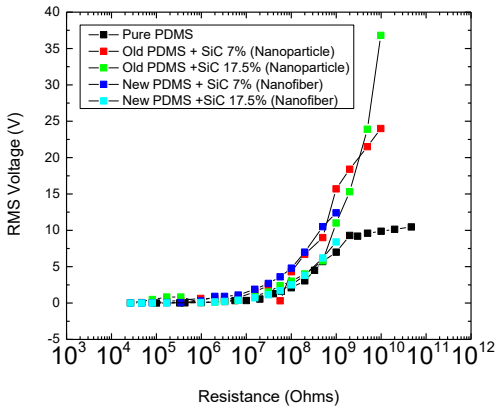

Figure 17: Load Voltage RMS

Load voltage for pure PDMS is measured at 10.46V with black peak in the graph. For PDMS with SiC 7% (nanoparticle), the red load voltage is peaked 24V, and PDMS with SiC 17.5% (green peak) has maximum value at 36.8V at higher resistance. In nanofibers, voltage blue peak drops to 12.4V for PDMS with SiC 7% and by further decreasing concentration to 17.5%, voltage drops to 8.4V. This might be because of increasing conductivity slightly but reducing the effective charge buildup needed for higher voltage generation. Moreover, open circuit voltage is measured when there no current flowing in the circuit and load voltage measured by applying R_L without applying weight unlike other samples (sample started sticking).

U(R) and I(R) in Figure 18 provide a general comparison between voltage and current. It shows the ideal behavior of voltage and current for the sample, and a point where U(R) and I(R) will superpose at resistance value to give power value.

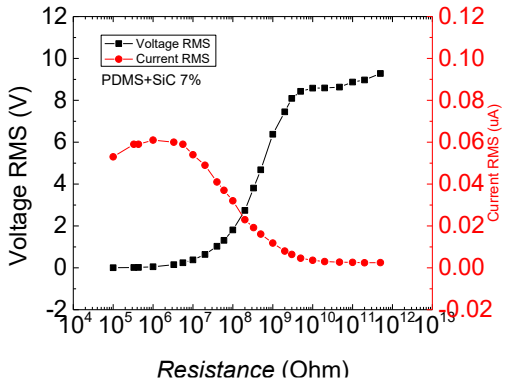

Figure 18: U(R) and I(R) Comparison for PDMS + SiC 7%

Calculated power density graph was plotted to check maximum power and maximum resistance. Following load voltage, highest power density values are obtained for pure PDMS at 3.249E-8 W/ cm^2. Among the three samples, lowest PD value is attained at 1.86323E-8 W/ cm^2. This happens when power is calculated using the formula.

$$P = \frac{V^2}{R} \qquad (5.4)$$

$$P.D = \frac{P}{2}\ W/cm^2 \qquad (5.5)$$

As illustrated above, power density can help find maximum load resistance. For this purpose, we took logarithm for power values, load resistance and applied polynomial equation on origin pro.

$$ax^2 + bx + c = 0 \qquad (5.6)$$

After applying polynomial equation, power parameter displaced in resultant sheet have intercept value as c, B1 as ax^2 and B2 bx value. By applying differentiation on polynomial equations.

$$x = \frac{-b}{2a} \qquad (5.7)$$

Now, by putting values B1 and B2, we will get x value for all three samples. After taking log of x, maximum resistance was derived shown in the table. Finding maximum resistance will find high resistance. the output power density increases gradually, Then, the output power density declines with the increasing resistance. The output reaches an optimal peak when the external load resistance matches the internal impedance of the device (Rload = Rinternal), after which it decreases at higher resistances due to restricted current flow.

Table 3: Maximum Power and Resistance

Samples	R_{max} (Ω)	P_{max} W
Pure PDMS	77.56 M	1.15 µ
PDMS + SiC_p 7%	8.85 M	0.41 µ
PDMS + SiC_p 17.5%	12.4 M	0.629 µ
PDMS + SiC_w 7%	5.6 M	5.6 µ
PDMS + SiC_w 17.5%	2.65 M	1.64 µ

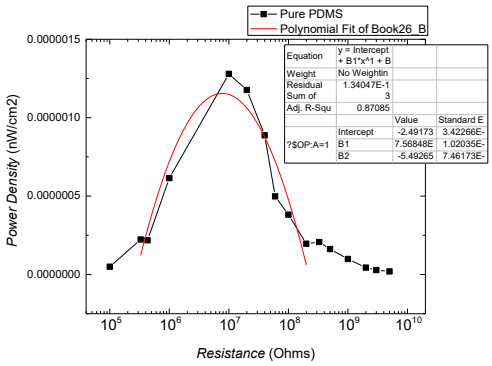

(a): Parabola Curve for Pure PDMS

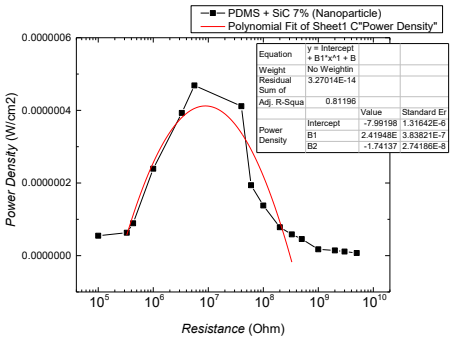

(b): Parabola Curve for PDMS + SiC_p 7%

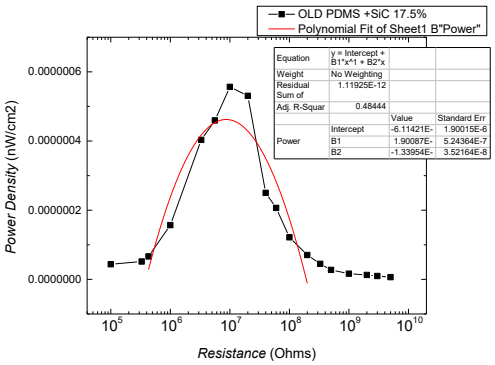

(c): Parabola Curve for PDMS + SiC_p 17.5%

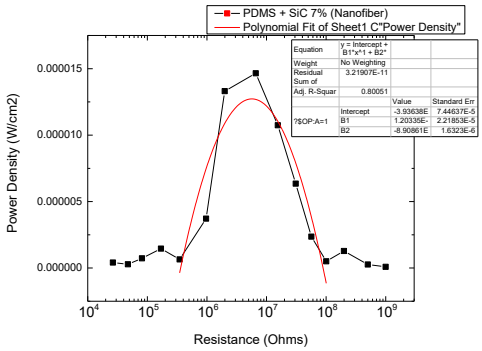

(d): Parabola Curve for PDMS + SiC_w 7%

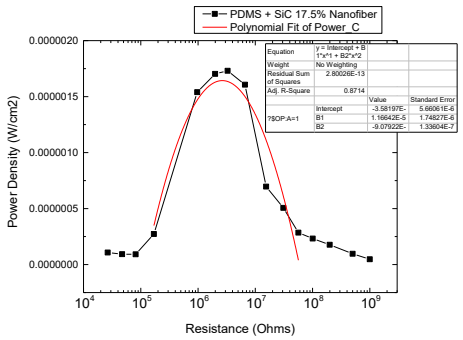

(e): Parabola Curve for PDMS + SiC_w 17.5%

Figure 19: Parabola Curves of prepared samples; (a): Parabola Curve for Pure PDMS; (b): Parabola Curve for PDMS + SiCp 7%; (c): Parabola Curve for PDMS + SiC_p 17.5%; (d): Parabola Curve for PDMS + SiC_w 7%; (e): Parabola Curve for PDMS + SiC_w 17.5%

The graph added above reflects that addition of SiC Nanofibers not only increases the total power output by nearly 500% compared to pure PDMS but also shifts the optimal operating point to a lower resistance range. This makes the PDMS /SiC_w 7% Nanofiber composite more suitable for powering standard low-power electronics which typically operate at lower impedances than pure polymers.

Measurement for capacitance is done on LCR meter connected with contact device. The measurements were taken with open and close contact. In open contact, capacitance is measured with air as a medium in between top contact (Al) and bottom contact (specified materials). In closed contact, capacitance is measured without any medium in between two top and bottom contact. Moreover, for closed contact different ranges of weights (345g, 942g and 1449g) for pure PDMS and PDMS /SiC_p. Whereas, for nanofibers, 507g weight was imposed on the contact device to study behavior. In open contact capacitance, total capacitance is CAIR. The graph below is frequency independent. In close contact, total capacitance is CPDMS. Capacitance formula is shown below.

$$c = \frac{\varepsilon_0 \varepsilon_r S}{d} \qquad (5.8)$$

Here, ε_0 is permittivity of free space, ε_r is relative permittivity, S surface charge density, d is distance between layers. In close contact, d becomes the thickness of substrate. Combined graphs of pure PDMS and with SiC in nanoparticles and nano whisker shown below in Figure 20, explaining how weak dielectric properties were in open contact when air is the effective gap d, and how close contact and at different weights enhances dielectric properties. Among all three

samples open contact capacitance exceeds nanofiber SiC 7% than pure PDMS and SiC 17.5% nanoparticle at 1.735E-12F. Since closed contact has different weights on it, for 345g capacitance enhanced to 2.20195E-11F at higher concentration of silicon carbide 17.5%. Increasing weight to 942g, capacitance reached to 2.35E-11F. At 1449g, capacitance peaked at 2.4008E-11F. Furthermore, nanofiber with SiC 7% obtained highest dielectric value at 1.71932E-12F for open contact and for closed contact, it reaches to 3.18725E-11F. Following nanofiber SiC 7%, SiC 17.5% has open contact dielectric value at 1.65005E-12F and closed contact dielectric at 3.68375E-11F. These experimental proofs depict that SiC particles and fibers successfully enhance the relative permittivity ($\boldsymbol{\varepsilon_r}$) of the PDMS matrix, acting as microscopic capacitors that store energy more effectively during the TENGs contact phase.

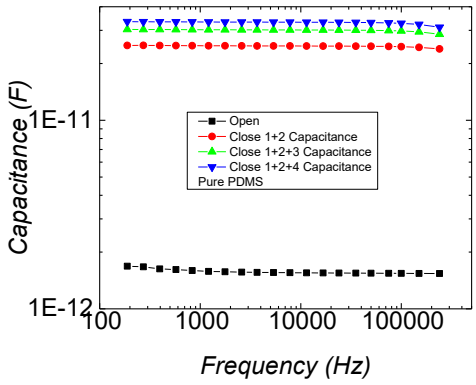

(a): Capacitance for Pure PDMS

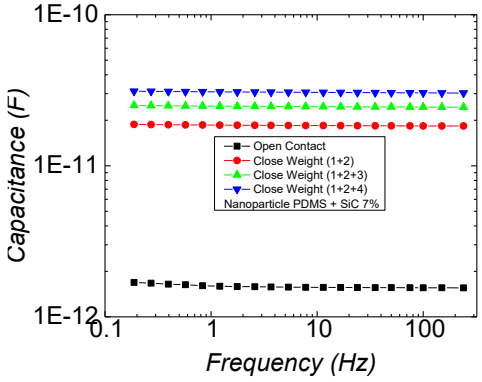

(b): Capacitance for PDMS + SiC_p 7%

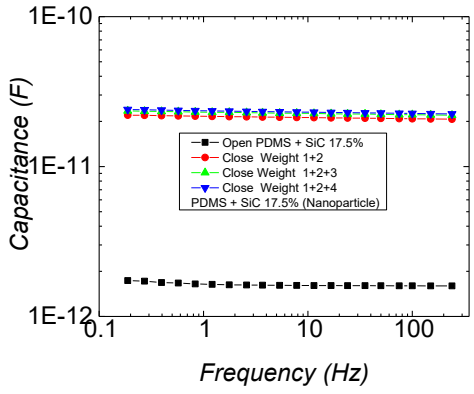

(c): Capacitance for PDMS + SiC_p 17.5%

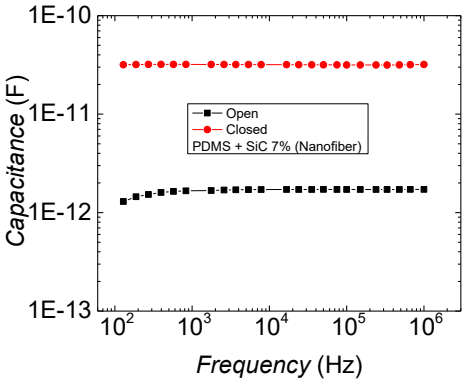

(d): Capacitance for PDMS + SiC_w 7%

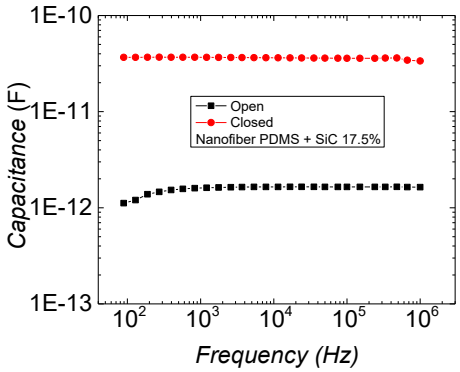

(e): Capacitance for PDMS + SiC_w 17.5%

Figure 20: Capacitance Graphs of prepared sample; (a): Capacitance for Pure PDMS; (b): Capacitance for PDMS /SiC_p 7%; (c): Capacitance for PDMS /SiC_p 17.5%; (d): Capacitance for PDMS /SiC_w 7%; (e): Capacitance for PDMS /SiC_w 17.5%

These findings align with Wang's fundamental theory that dielectric engineering is the key to overcoming the "output bottleneck" of polymers. The recorded voltage of ~67.5 V follows the theoretical trends predicted in the 2012-2021 TENG models. Plyushch's "percolation threshold" theory predicted that nanofibers/whiskers would outperform nanoparticles due to high-aspect-ratio geometry. My work also proposed that silicon carbide drops in performance at 17.5%. This proof the Kim's findings that excessive filler leads to increased leakage current, identifying 7% as a more balanced "golden ratio" for power harvesting.

The decreased performance of TENG at higher concentration of silicon carbide suggests percolation (leakage mechanism), but dielectric loss should be measured to confirm leakage mechanism. The superior performance of the 7% Nanofiber sample is facilitating greater Maxwell-Wagner polarization compared to nanoparticles. Similarly, the performance drop at 17.5% can be attributed to the lower percolation threshold of the nanofibers, which eventually promotes internal charge leakage.

Table 4: Achieved Maximum Results

Metric	**Pure PDMS**	**SiC_p 7 wt%**	**SiC_w 7 wt%**
Max. Voc (V)	83	70.9	93.442
Charge nC/cm^2	1.64	2.04	2.56
P^{max} for samples (W)	1.15	0.41	5.6

5.2 PDMS/SiCw Composites:

Following distinction performance of PDMS /SiC_w 7% research shifted toward nano whisker and to achieve optimum results, PDMS with diverse amount of silicon carbide from (.5 wt% to 35wt% were prepared as the method is illustrated above and their short circuit current characteristics were analyzed. Among all the 8 nano whisker samples mentioned in Figure 21, compared with black peaks which represent pure PDMS, highest pink peak obtained with 14 wt% concentration of silicon carbide at 4.58008µA, followed by blue peak representing PDMS /SiC_w with 10 wt % at 4.0332µA. The lowest short circuit current is achieved at red peaks for 3.5 wt% of silicon carbide at 1.04395µA. These peaks also suggest that with increment of silicon carbide to polydimethylsiloxane certainly decreases short circuit current at 35wt%.

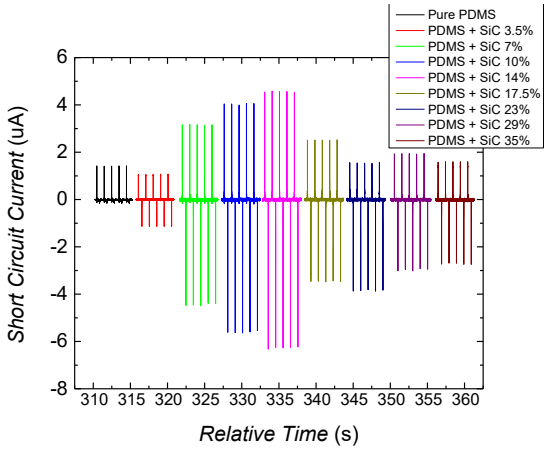

Figure 21: Short Circuit Current

After observing the rate of flow charge among nine samples of nano whiskers, surface charge is obtained through TENG device using Aluminum as an electrode. Since nano whiskers showed significant results, surface charges values retrieved from whiskers gave highest surface charge deposition for 14 wt% incorporation of silicon carbide to polydimethylsiloxane at 4.63721 nC/cm^2 and negative surface charge at -5.59521 nC/cm^2, thereafter comes 10 wt% with positive surface charge at 4.36768 nC/cm^2 and negative charge values at -5.28516nC/cm^2. The increase of impurity brought decrease of the surface charge. The lowest concentration of 3.5 wt% also brought lowest positive and negative value of charges taken over relative time.

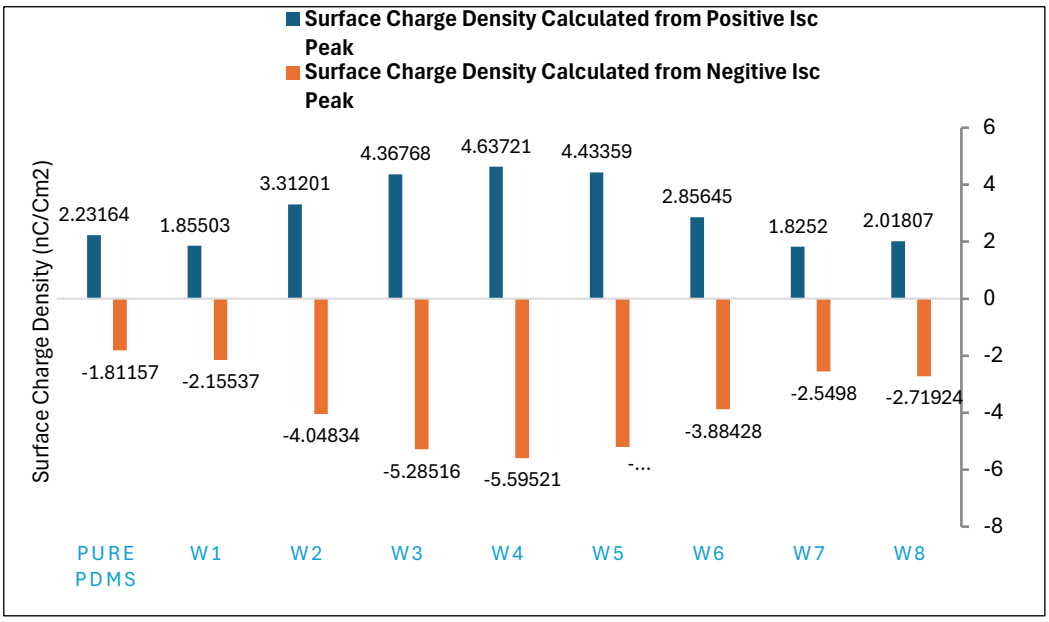

Figure 22: Surface Charge Density

Table 5: Surface Charge Density of Nano whiskers

Samples wt %	Q(+ve) nC/cm2	Q(-ve) nC/cm2
Pure PDMS	2.23164	-1.81157
W1	1.85503	-2.15537
W2	3.31201	-4.04834
W3	4.36768	-5.28516
W4	4.63721	-5.59521
W5	4.43359	-5.20654
W6	2.85645	-3.88428
W7	1.8252	-2.5498
W8	2.01807	-2.71924

The graphs in Figure 22 proposed that addition of fillers increases the dielectric permittivity of PDMS and hence surface charge also increases, but after a certain addition it can also transit from insulator to conductive pathway. This could be the reason that 27 wt% to 35 wt% the surface charge consecutively dropped. Therefore, the sample range for observance is restricted to PDMS /SiC_w 23%, and U_{LOAD} and I_{LOAD} graphs are shown in figure 22 and 23 below. The curves in Figures 23 and 24 follow the ideal

behavior of voltage and current with varying load. Highest load voltage is achieved for PDMS /SiC_w 14 wt% at 31.2V, with the lowest voltage of 5.63V at highest resistance achieved for silicon carbide with 17.5 wt% concentration. In contrast, nano whiskers load current graphs points peak current performance for 17.5 wt% 0.28 µA followed by 14 wt% with load current valued at 0.26 µA. The grotesque peaks of 17.5 wt% are because lower capacitance and internal charge leakage dropped voltage at high resistance. While in load current, surface charge density boosted at low external resistance.

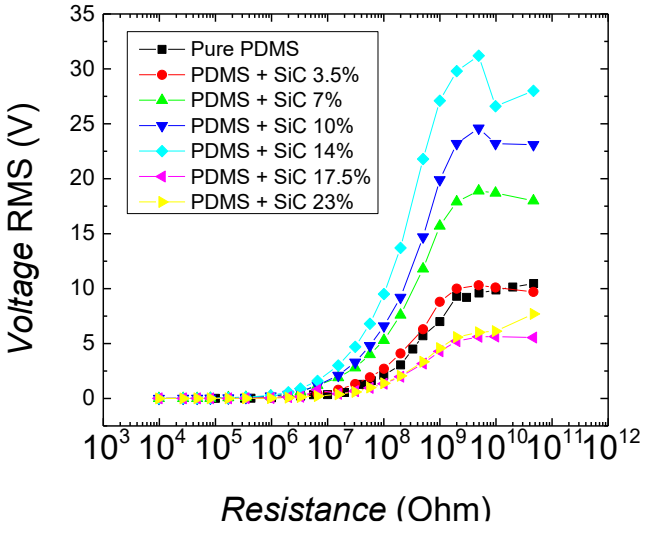

Figure 23: Load Voltage for Nano Whiskers

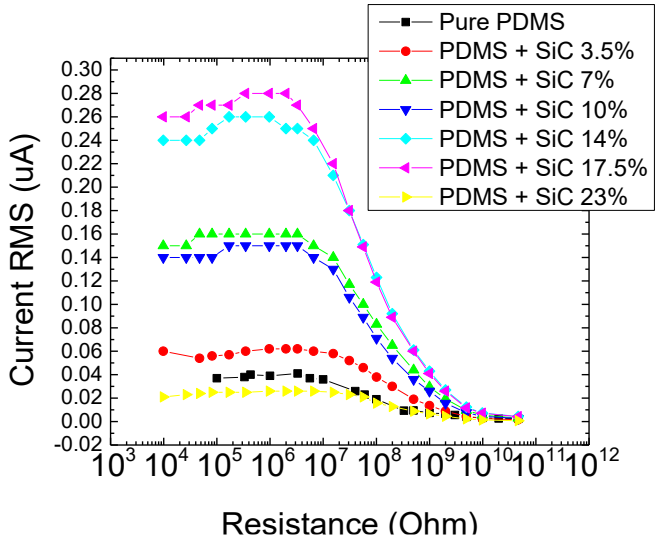

Figure 24: Load Current for Nano Whiskers

To calculate power, ($P = \frac{V^2}{R}$) is applied individually to measured data. Here, voltage measured over relative time and R represents individual resistive load of the sample. This power is integrated to find areas under power curve and to calculate exact energy produced.

$$A_0 = \int_{x_1}^{x_2} P_{inst}(t)\, dt \qquad (5.9)$$

$$P_{avg} = \frac{A_0}{x_2 - x_1} \qquad (5.10)$$

Here, equations are used to calculate areas under the instantaneous power curve between beginning of time x1 and ending time x2. And equation is used to calculate average power over certain time of the curve. Power densities of prepared whiskers are plotted and shown in Figurs 25. Figure 26 presents maximum power measured at optimal resistance for pure PDMS and whisker samples. As it is visible in Figure 24, all the curves show symmetrical and bell-shaped distribution of graphs over resistance. hence, gaussian method is utilized, which is a non-linear square curve method. It comprises of three characteristics, optimal internal resistance, energy production showing peak area and baseline noise. Gaussian method equation is mentioned below;

$$y = y_0 + \frac{A}{\omega\sqrt{\frac{\pi}{2}}} exp[-2\left(\frac{x - x_C}{\omega}\right)^2] \qquad (5.11)$$

Where, y is power density in W/cm^2, x is logarithm of load resistance, y_0 is baseline offset, x_C is peak center (optimal resistance value), ω is width of peak and A is area. Maximum power is calculated at 1.30922E-5 W/cm^2 for PDMS /SiC_w 14wt% with optimal resistance of 10.36096 MΩ, using data after applying gaussian method mentioned below;

$$R^{max} = 10^{x_c} \qquad (5.12)$$

$$P.d = y_0 + A \qquad (5.13)$$

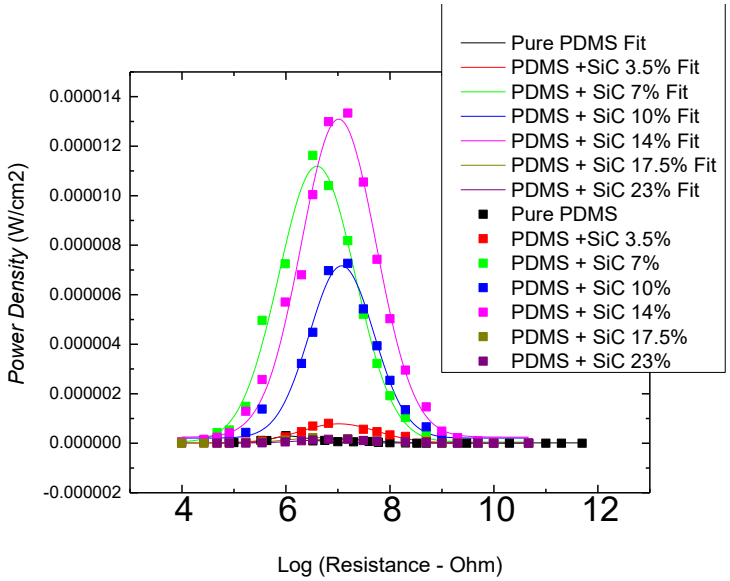

Figure 25: Power Density Combined

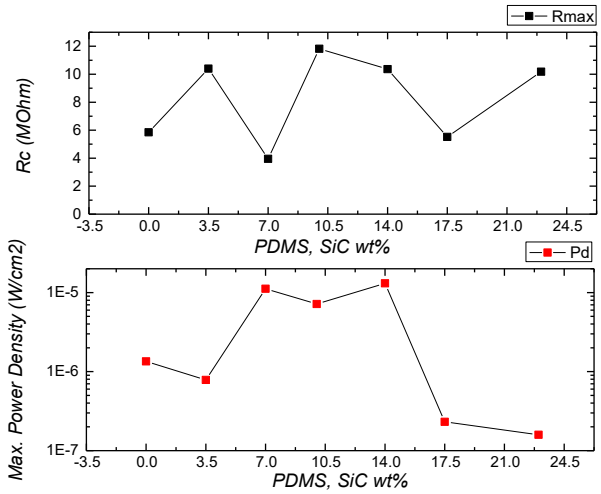

Figure 26: R^{max} and P^{max} Combined

Table 5: R^{max} and P^{max} of Pure PDMS and PDMS/SiC Nano whiskers

Samples **wt %**	**Rmax** **Mohm**	**P.d** **W/cm2**
Pure PDMS	5.85	1.34750E-6
3.5	10.4	7.8464E-7
7	3.95594	1.11901E-5
10	11.82	7.16593E-6
14	10.36096	1.30922E-5

17.5	5.52154	2.3198E-7
23	10.18474	1.589E-7

To observe dielectric behavior of prepared sample, capacitance is measured on impedance meter (Solartron Modulable XM MTS System) connected to vertical contact separation device. The impedance meter is set at a frequency range of 100 Hz to 1 MHz, and the capacitance is measured likewise the previous (in open and closed contact). In case of closed contact for prepared sample (Pure PDMS and PDMS /SiC_w from 3.5 wt% to 23 wt%), capacitance is measured by applying 0N and 11N weight. Impedence meter with under certain characteristics measured capacitance in open contact, and the formulas used to calculate capacitance are mentioned below;

$$\boldsymbol{\Delta C = C_{11N} - C_{0N}} \qquad \textbf{(5.14)}$$

$$\boldsymbol{\Delta C_{max.} = C_{11N} - C_{Open}} \qquad \textbf{(5.15)}$$

Here, $\boldsymbol{\Delta C_{max.}}$ is used to calculate capacitance of prepared samples in open contact. In this case, air is used as a medium between electrode and bottom contact with digital oscilloscope set at 11N force. Since the medium is air, therefore capacitance measured at 11N in closed contact is subtracted with $\boldsymbol{C_{Open}}$. In close contact, Capacitance measured in closed at 11N expanded the surface of the bottom contact and hence charge storage increase in comparison with open contact and $\boldsymbol{C_{0N}}$ in close contact. Furthermore, for calculation of prepared samples, $\boldsymbol{C_{11N}}$, $\boldsymbol{C_{0N}}$ and $\boldsymbol{C_{Open}}$ taken at frequency of 100 Hz. And the Figure 27 mentioned below, graph (a) explains how higher concentration of silicon carbide enhances capacitance open contact. here, air makes the top electrode and bottom contact act two capacitors in series, and store charges as dielectric permittivity improves. whereas graph (b) shows that quantity of silicon carbide to polydimethylsiloxane can increase or decrease its capacitance by transitioning it from insulator to a conductor. When two surfaces are pressed, more SiC particles come into contact and form a conductive pathway.

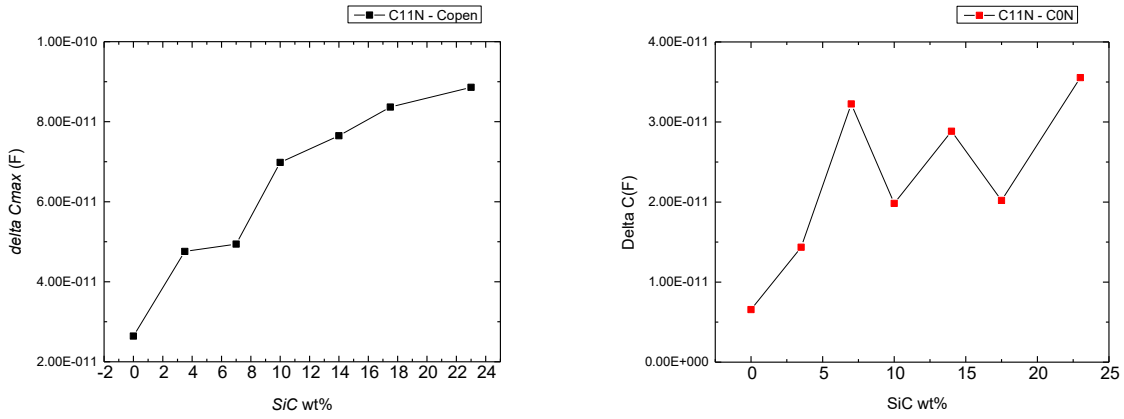

(a): Capacitance in Open Contact (b): Capacitance in Closed Contact

Figure 27: Capacitance of Pure PDMS and PDMS/SiC of prepared samles; (a): Capacitance in Open Contact(b): Capacitance in Closed Contact

6: Conclusions

The investigation of triboelectric properties of PDMS/SiC concludes:

1. PDMS /SiC_w showed higher potential to trap charges (V_{oc} at 93.42V), (Q_{SC}) of 2.56 nC/cm², and P^{max} at 5.6μ W, in comparison with PDMS /SiC_p V_{oc} lower than pure PDMS (83V),

2. Among PDMS /SiC_w ranging from 3.5 to 35 wt% showed Q_{SC} enhancing at 14 wt% 4.64 nC/cm², and I at 4.58 μA. Study showed that further incorporation caused internal charged leakage.

3. Structured review of PDMS/SiC_w gave 31.2 V and $P.d^{max}$ at 13.09 μW/cm^2 under variable external resistance. Moreover, with increased concentration, stress regulates internal capacitance in close contact.

7. References

1. Wang ZL. Triboelectric nanogenerators as new energy technology for self-powered systems and as active mechanical and chemical sensors. ACS nano. 2013 Nov 26;7(11):9533-57. https://doi.org/10.1021/nn404614z

2. X.He, Y.Zi, H.Guo, H.Zheng, Y.Xi, C.Wu, J.Wang, W.Zhang, C.Lu, Z. L.Wang, Adv. Funct. Mater.2017, 27, 1604378.. https://doi.org/10.1002/adfm.201604378

3. He D, Wang Y, Song S, Liu S, Deng Y. Significantly enhanced dielectric performances and high thermal conductivity in poly (vinylidene fluoride)-based composites enabled by SiC@ SiO2 core–shell whiskers alignment. ACS applied materials & interfaces. 2017 Dec 27;9(51):44839-46. https://doi.org/10.1021/acsami.7b14751

4. Zhao, K., Sun, W., Li, S. *et al.* Rational design on high-performance triboelectric nanogenerator consisting of silicon carbide@silicon dioxide nanowhiskers/polydimethylsiloxane ($SiC@SiO_2$/PDMS) nanocomposite films. *Discover Nano* 18, 69 (2023). https://doi.org/10.1186/s11671-023-03822-8

5. Kim MP, Lee G, Noh B, Kim J, Kwak MS, Lee KJ, Ko H. Enhancing energy harvesting performance of bilayered parylene triboelectric nanogenerators through interfacial polarization. Nano Energy. 2024 Jan 1;119:109087. 10.1016/j.nanoen.2023.109087

6. Wang, Y., Yang, Y. & Wang, Z.L. Triboelectric nanogenerators as flexible power sources. *npj Flex Electron* 1, 10 (2017). https://doi.org/10.1038/s41528-017-0007-8

7. Wang ZL. From contact electrification to triboelectric nanogenerators. Reports on Progress in Physics. 2021 Sep 7;84(9):096502. Zhong Lin Wang 2021 *Rep. Prog. Phys.* 84 096502 DOI 10.1088/1361-6633/ac0a50

8. Luo J, Wang ZL. Recent progress of triboelectric nanogenerators: From fundamental theory to practical applications. EcoMat. 2020;2:e12059. https://doi.org/10.1002/eom2.12059

9. C.Xu, Y.Zi, A. C.Wang, H.Zou, Y.Dai, X.He, P.Wang, Y.-C.Wang, P.Feng, D.Li, Z. L.Wang, Adv. Mater.2018, 30, 1706790. https://doi.org/10.1002/adma.201706790

10. Shao J, Willatzen M, Wang ZL. Theoretical modeling of triboelectric nanogenerators (TENGs). Journal of Applied Physics. 2020 Sep 21;128(11). https://doi.org/10.1063/5.0020961

11. Thadikkal Abdul Muthalif, N., Al Rashid, A. & Koç, M. (2026). Nanogenerators for energy harvesting: a holistic review of mechanisms, materials, and emerging applications. *Nanotechnology Reviews*, *15*(1), 20250268. https://doi.org/10.1515/ntrev-2025-0268

12. Niu, S., Liu, Y., Wang, S., Lin, L., Zhou, Y.S., Hu, Y. and Wang, Z.L. (2013), Theory of Sliding-Mode Triboelectric Nanogenerators. Adv. Mater., 25: 6184-6193. https://doi.org/10.1002/adma.201302808

13. Cao, L. N. Y., Xu, Z., & Wang, Z. L. (2022). Application of Triboelectric Nanogenerator in Fluid Dynamics Sensing: Past and Future. *Nanomaterials*, *12*(19), 3261. https://doi.org/10.3390/nano12193261

14. Nurmakanov, Y., Kalimuldina, G., Nauryzbayev, G. *et al.* Structural and Chemical Modifications Towards High-Performance of Triboelectric Nanogenerators. *Nanoscale Res Lett* 16, 122 (2021). https://doi.org/10.1186/s11671-021-03578-z

15. A.Šutka, L.Lapčinskis, D.He, H.Kim, J. D.Berry, J.Bai, M.Knite, A. V.Ellis, C. K.Jeong, P. C.Sherrell, Engineering Polymer Interfaces: A Review toward Controlling Triboelectric Surface Charge. Adv. Mater. Interfaces2023, 10, 2300323. https://doi.org/10.1002/admi.202300323

16. Niu, S., Wang, S., Lin, L., Liu, Y., Zhou, Y. S., Hu, Y., & Wang, Z. L. (2013). Theoretical study of contact-mode triboelectric nanogenerators as an effective power source. *Energy & Environmental Science*, *6*(12), 3576-3583.

17. Zhang R, Olin H. Material choices for triboelectric nanogenerators: A critical review. EcoMat. 2020;2:e12062. https://doi.org/10.1002/eom2.12062

18. Machín A, Fontánez K, Arango JC, Ortiz D, De León J, Pinilla S, Nicolosi V, Petrescu FI, Morant C, Márquez F. One-Dimensional (1D) Nanostructured Materials for Energy Applications. *Materials*. 2021; 14(10):2609. https://doi.org/10.3390/ma14102609

19. Y.Liu, J.Ping, Y.Ying, Recent Progress in 2D-Nanomaterial-Based Triboelectric Nanogenerators. Adv. Funct. Mater.2021, 31, 2009994. https://doi.org/10.1002/adfm.202009994

20. T.Xu, J.Ye, J.-C.Tan, Unravelling the Ageing Effects of PDMS-Based Triboelectric Nanogenerators. Adv. Mater. Interfaces2024, 11, 2400094. https://doi.org/10.1002/admi.202400094

21. Kim, D.W., Lee, J.H., Kim, J.K. *et al.* Material aspects of triboelectric energy generation and sensors. *NPG Asia Mater* 12, 6 (2020). https://doi.org/10.1038/s41427-019-0176-0

22. X.Liu, E.Sun, H.Yang, X.Cao, and N.Wang, "Fiber-Reinforced Composites for High-Performance Triboelectric Nanogenerators: Materials Design, Manufacturing Innovations, and Emerging Applications." Small21, no. 51 (2025): e08547. https://doi.org/10.1002/smll.202508547

23. Sigma-Aldrich. (2026). SYLGARD® 184 silicone elastomer kit (Cat. No. 761036). Merck. https://www.sigmaaldrich.com/

24. Han J, Yang X, Liao L, Zhou G, Wang G, Xu C, Hu W, Debora ME, Song Q. Photoinduced triboelectric polarity reversal and enhancement of a new metal/semiconductor triboelectric nanogenerator. Nano Energy. 2019 Apr 1;58:331-7. 10.1016/j.nanoen.2019.01.019

25. Karchung -, Sabrina Schaly, Alistair McEwan, et al. Self-Powered Wearables: Material Innovations Driving Triboelectric Nanogenerators. *Authorea*. 06 August 2025.
DOI: https://doi.org/10.22541/au.175447812.29680019/v1

8. Summary

Triboelektriniai nanogeneratoriai (TENG) yra perspektyvūs įrenginiai, skirti žemo dažnio mechaniniam judėjimui paversti elektros energija, skirta savarankiškai maitinamiems jutikliams, nešiojamai elektronikai ir daiktų interneto taikymams. PDMS plačiai naudojamas TENG dėl savo lankstumo, cheminio stabilumo ir lengvo gamybos, tačiau maža dielektrinė konstanta riboja krūvio kaupimą ir išvesties našumą. Šiame darbe buvo tiriamos PDMS/SiC kompozicinės plėvelės, siekiant įvertinti, kaip SiC morfologija ir koncentracija veikia TENG veikimą. Gryni PDMS, PDMS/SiCp kompozitai ir PDMS/SiCw kompozitai buvo paruošti ant ITO-PET substratų ir išbandyti vertikaliu kontaktiniu atskyrimo režimu, naudojant aliuminį kaip priešpriešinį elektrodą. Mėginiai buvo analizuojami atliekant atviros grandinės įtampos, trumpojo jungimo srovės, paviršiaus krūvio tankio, galios tankio ir talpos matavimus.

Rezultatai parodė, kad SiCw efektyviau pagerino PDMS pagrindu sukurto TENG veikimą nei SiCp. Morfologijos palyginime 17,5 % masės SiCw mėginys sukūrė didžiausią atviros grandinės įtampą –

apie 93,42 V, o 7 % masės SiCw mėginys pasižymėjo dideliu krūvio tankiu ir apkrovai pritaikyta galia. Išplėstinėje „ūsų“ serijoje optimalus našumas buvo pasiektas esant 14 % masės, kai trumpojo jungimo srovė buvo apie 4,58 μA, krūvio tankis – 4,64 nC/cm², o maksimalus galios tankis – 13,09 μW/cm². Apskritai optimizuoti PDMS/SiCw kompozitai tinka lanksčiams TENG, naudojamiems nešiojamuosiuose ir daiktų interneto (IoT) autonominio maitinimo jutikliuose.

Triboelectric nanogenerators (TENGs) are promising devices for converting low-frequency mechanical motion into electrical energy for self-powered sensors, wearable electronics, and IoT applications. PDMS is widely used in TENGs because of its flexibility, chemical stability, and ease of fabrication, but its low dielectric constant limits charge storage and output performance. This work investigated PDMS/SiC composite films to evaluate how SiC morphology and concentration affect TENG performance. Pure PDMS, PDMS/SiCp composites, and PDMS/SiC_w composites were prepared on ITO-PET substrates and tested in vertical contact-separation mode using aluminum as the counter-electrode. The samples were analyzed through open circuit voltage, short circuit current, surface charge density, power density, and capacitance measurements.

The results showed that SiC_w improved PDMS-based TENG performance effectively than SiC_p. In the morphology comparison, the 17.5 wt% SiC_w sample produced the highest open-circuit voltage of about 93.42 V, while 7 wt% SiC_w showed high charge density and load-matched power. In the extended whisker series, the optimum performance was obtained at 14 wt%, with a short-circuit current of about 4.58 μA, charge density of 4.64 nC/cm², and maximum power density of 13.09 μW/cm². Overall, optimized PDMS/SiC_w composites are suitable for flexible TENGs in wearable and IoT self-powered sensors.